American Mineralogist, Volume 84, pages 838–847, 1999

Crystal-chemical controls on trace element partitioning between garnet and anhydrous silicate melt

WIM VAN WESTRENEN,* JON BLUNDY, AND BERNARD WOOD

CETSEI, Department of Earth Sciences, University of Bristol, Wills Memorial Building, Bristol BS8 1RJ, U.K.

ABSTRACT

We performed experiments at 3.0 GPa and 1530–1565 °C to investigate the effects of crystal composition on trace element partitioning between garnet and anhydrous silicate melt. Bulk compositions along the pyrope (Py: $Mg_3Al_2Si_3O_{12}$)-grossular (Gr: $Ca_3Al_2Si_3O_{12}$) join, doped with a suite of trace elements (Li, B, K, Sc, Ti, Sr, Y, Zr, Nb, Cd, In, REE, Hf, Ta, Th, and U) produced homogeneous garnets, ranging in composition from $Py_{84}Gr_{16}$ to Py_9Gr_{91}, in equilibrium with melt.

Trace element partition coefficients (*D*-values), measured by SIMS, depend greatly on the Mg/(Mg + Ca) of garnet. For example, from Py_{84} to Py_9, D_{La} increases from 0.004 to 0.2, whereas D_U increases from 0.029 to 0.42. These variations can be explained by the lattice strain model of Blundy and Wood (1994), which describes trace element partitioning of an element *i* in terms of the ionic radius of *i* (r_i), the size of the lattice site on which *i* partitions (r_0), the Young's modulus of the site (E), and the (theoretical) partition coefficient D_0 for an ion of radius r_0.

For trivalent cations substituting in the garnet X-site (Y, REE, Sc, and In), apparent values of r_0 fitted to our data vary systematically from 0.935 ± 0.004 Å (Py_{84}) to 0.99 ± 0.01 Å (Py_9), a trend consistent with variations in the size of the X-site. Values of D_0 show an increase from Py_9 (D_0 = 2.8 ± 0.1) to Py_{84} (4.8 ± 0.1) and Young's modulus E varies from 257 ± 20 GPa for Py_{60} to 590 ± 40 GPa for Py_{84}. These results allow a quantitative assessment of the influence of crystal chemistry on garnet-melt *D*-values, thereby forming the basis for a predictive model similar to that recently developed for clinopyroxene-melt partitioning by Wood and Blundy (1997). Our new data emphasize the importance of taking into account crystal composition when modeling trace element behavior in natural systems.

INTRODUCTION

Several lines of geochemical evidence, such as U-Th isotopic disequilibrium and Sm-Nd and Lu-Hf isotope systematics in MORB, point toward an important role for garnet in the mantle melting region (e.g., Salters and Hart 1989; Beattie 1993; LaTourrette et al. 1993; Salters 1996). The evidence supporting this interpretation is based largely on the ability of garnet to incorporate certain trace elements preferentially over others, as derived from a limited number of high-pressure, high-temperature partitioning experiments. In fact, all of the existing geochemical models of mantle melting are predicated on assumptions about differences in partitioning behavior between garnet and clinopyroxene, assumptions that have been called into question recently (Blundy et al. 1998). Since the existing garnet/melt partitioning data set does not cover a wide range in pressure (P), temperature (T), and bulk composition (X), it is impossible to take into account the effects of these intensive parameters on garnet-melt partition coefficients during the melting process. Most geochemical models are, therefore, based on fixed, constant garnet/melt partition coefficients measured under one set of "appropriate" conditions. This approach, as shown by Blundy and Brodie (1997), can cause large errors in modeling of mantle melting processes.

There is, therefore, a need for *systematic* studies of garnet/melt partitioning, isolating where possible the effects of P, T, and X (and f_{O_2} in the case of polyvalent cations). The purpose of this study was to determine specifically the role that crystal chemistry plays in controlling the partitioning between garnet and anhydrous silicate melt. Experiments were performed in the simple system CaO-MgO-Al_2O_3-SiO_2 (CMAS) under isobaric (3.0 GPa), near-isothermal (1530–1565 °C) conditions to isolate the effect of Mg/(Mg + Ca) ratio. We show for the first time a systematic dependence of *D*-values on garnet composition along the pyrope-grossular join. Although our experiments were performed in a simple system, our results have important implications for future models of garnet/melt partitioning applicable to natural systems.

METHODS

Starting materials and experimental setup

Starting materials with compositions $Mg_3Al_2Si_3O_{12}$ and $Ca_3Al_2Si_3O_{12}$ were prepared by mixing appropriate proportions of analytical grade oxides (for Mg, Al, and Si) and carbonate (for Ca). The pyrope oxide mix was first heated in a platinum crucible from 800–1300 °C, then ground under ethanol in an agate mortar used previously for Fe-free materials only. The grossular mix was twice heated slowly from 650–1300 °C (ground under ethanol after each heating cycle) to ensure full decarbonation. Subsequently both starting mixes were heated

*E-mail: W.van-Westrenen@bristol.ac.uk

at 1300 °C for 24 h to remove any remaining adsorbed water and CO_2. To re-create the garnet/melt relations at 3.0 GPa reported by Walter and Presnall (1994) and Maaløe and Wyllie (1979) we then prepared the following mixtures: $Py_{82}Gr_{18}$ (mixture G1); $Py_{50}Gr_{50}$ (G3); and $Py_{15}Gr_{85}$ (G4). In addition, a mixture G2 was prepared with a composition close to the melt composition generated by Walter and Presnall (1994) in their experiment 562-1.

Atomic Absorption standard solutions containing 1000 ppm each of the element of interest were used to dope mixtures G2, G3, and G4 with a suite of 26 trace elements (see Table 1 for details) chosen so as to minimize molecular interferences in ionprobe analysis. Total dopant levels were limited to 0.14–0.51 wt% (Table 1). After drying at room temperature all doped mixtures were kept at 110 °C until use.

The experimental arrangement is shown in Figure 1. All samples were loaded into graphite capsules fitted tightly inside 2 mm O.D. platinum capsules. To assess the influence of the graphite liner, one experiment was performed in a platinum capsule only (see Table 2). Before welding, all capsules were held at 760 °C for 10 min to drive off any adsorbed water. The welded capsule was then embedded in a crushable alumina cylinder and covered with a thin platinum disk to protect it from the W-3%Re/W-25%Re thermocouple. Surrounding parts consist of a graphite furnace, a silica glass inner sleeve to increase quench rates, and a $BaCO_3$ outer sleeve. The vertical temperature gradient across the capsule is on the order of 10 °C (Frost and Wood 1997).

A pressure calibration was performed for this cell using 50:50 mixtures of pyrope and enstatite plus 3 wt% PbO flux. These were run at nominal pressures of 2.5–3.3 GPa and temperatures of 1300–1600 °C. Measured Al_2O_3 contents of the resulting enstatite were compared with data of Perkins et al. (1981). The resulting pressure correction at our run temperatures is –13 ± 1%. No correction was made for the dependence of thermocouple emf on pressure. During heating to run temperature, pressure was increased continuously, the last increment of pressure being applied after the run temperature had

TABLE 1. Major and trace element compositions of starting materials

	G1*		G2†		G3†		G4†	
Oxides	Comp.	σ	Comp.	σ	Comp.	σ	Comp.	σ
CaO	5.4	0.1	13.7	0.1	18.5	0.1	31.6	0.3
MgO	25.2	0.4	21.8	0.1	15.0	0.1	4.4	0.1
Al_2O_3	25.2	0.2	16.7	0.1	23.8	0.1	22.8	0.2
SiO_2	44.2	0.3	47.7	0.4	42.8	0.2	40.8	0.2
Total	100.0	0.4	100.0	0.6	100.1	0.3	99.6	0.3
Trace elements								
Li			21.1	0.5	18.4	0.2	21.6	0.4
B			388	9	345	4		
K			2103	122	1590	151	723	106
Sc			16.6	1.4	15.0	0.4	20.2	0.5
Ti			49.0	5.3	23.5	0.9	24.1	0.6
Sr			134	4	158	3	244	5
Y			8.6	0.5	15.2	0.3	16.9	0.3
Zr			18.0	1.0	19.4	1.0	24.3	1.0
Nb			22.6	1.7	31.3	1.5	18.1	0.6
Cd			357	145	118	14	18.4	4.7
In			414	21	377	9	23.3	3.0
La			55.2	2.7	36.8	0.6	44.1	0.6
Pr			14.7	0.8	10.7	0.3	15.1	0.3
Sm			10.2	0.6	11.2	0.6	16.2	0.5
Tb			10.2	0.6	11.1	0.2	12.5	0.3
Er			10.5	0.5	11.1	0.2	37.4	0.9
Tm			10.4	0.4				
Yb			9.3	0.5	10.4	0.3	13.8	0.4
Lu			4.8	0.5	10.8		13.9	0.3
Hf			9.8	1.6	11.0	1.2	12.9	0.7
Ta			400	79	31.9	3.8	25.1	1.2
Th			885	73	736	25	88.9	2.3
U			152	11	139	4	28.2	1.0
Total			5104	219	3734	154	1442	106

Note: Oxides in weight percent; trace elements in parts per million.
* Major element data taken from Walter and Presnall (1994).
† Approximately 10 mg of starting material was fused for 30 min in a welded platinum capsule at 1520 °C and 1 atm pressure, and subsequently quenched in water.

TABLE 2. Experimental conditions and products

Details	8	11	12	13	14
Starting material	20 wt%G1, 80 wt%G2	See exp. 8	G3	G4	G3
Capsule(s)	Pt	C + Pt	C + Pt	C + Pt	C + Pt
P (kbar)	30	30	30	30	30
T (°C)	1560	1565	1545	1530	1530
t (h)	21	21	21	22	21
Products (wt%)	gt (35) q (65) px (trace)	gt (36) gl+q (64) px (trace)	gt (43) q (57)	gt (67) q (33)	gt (55) q (45)

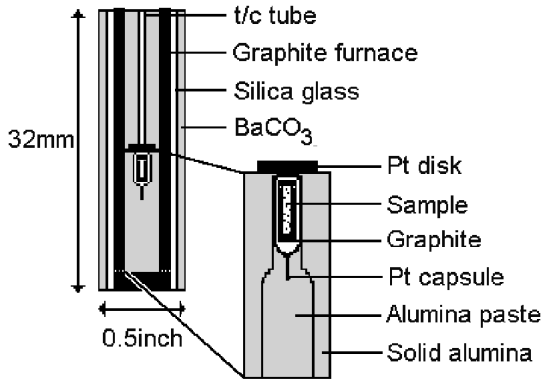

FIGURE 1. Experimental setup—see text for details; t/c is a W-3%Re/W-25%Re thermocouple.

been reached (hot-piston-in technique). Experimental conditions and durations are shown in Table 2.

Analytical techniques

Major element compositions of starting materials and experimental products were determined with the JEOL 8600 Superprobe at Bristol University, using an accelerating voltage of 15 kV and a beam current of 15 nA. A focused beam with a 1 mm spot size was used for garnet analyses, whereas a layer spot size (10 mm) was used for analyses of quench crystals and glass. Counting times were 30 s for all four elements. Standards used were wollastonite for Si and Ca, spinel for Al, and olivine for Mg. Analyses of secondary standards (including diopside, KK1 kaersutite, Kakanui garnet, and natural pyrope) were consistently within 2s of published values.

Trace elements were measured on Au-coated mounts with the Cameca IMS-4f ion microprobe at Edinburgh University. The primary beam was 10.69 kV O^- ions with 8–10 nA beam current, focused to a ~20 μm spot. To reduce transmission of molecular ion species an offset of 73 ± 20 eV was applied to the secondary ion accelerating voltage of 4.5 keV. The energy window was set to 20 eV. Isotopes ^{7}Li, ^{11}B, ^{41}K, ^{42}Ca, ^{44}Ca, ^{45}Sc, ^{47}Ti, ^{88}Sr, ^{89}Y, ^{90}Zr, ^{93}Nb, ^{114}Cd, ^{115}In, ^{139}La, ^{141}Pr, ^{149}Sm, ^{159}Tb, ^{167}Er, ^{169}Tm, ^{172}Yb, ^{175}Lu, ^{178}Hf, ^{181}Ta, ^{232}Th, and ^{238}U were measured and ratioed to ^{30}Si, after calibration on NIST standard SRM610. Mass 130.5 was used to monitor background; all analyses reported here have zero background counts. Counting times were adjusted so as to obtain at least 10^3 total counts per isotope and, for analyses consisting of 10 cycles, were typically around 5 s per cycle for elements present at the parts per million level.

Accuracy of the SIMS analyses was assessed by analyzing regularly a set of secondary standards: basalt glasses BIR-1 (Jochum et al. 1990) and BCR-1 (Govindaraju 1994); Irving and Frey (1978) garnet DD1; and Mongolian garnet MU5388 (Norman et al. 1996). Table 3 and Figure 2 compare published trace element compositions with values measured by us over a period of 4 years. Figure 2 shows accuracy for all elements is generally better than 15% and better than 10% for most REE. More importantly, where available for both garnet and glass standards, ratios observed to published data overlap within error for all elements except Sr, Y, and La (for a discussion of these exceptions see legend of Fig. 2). The absence of differential matrix effects for glass relative to garnet means the accuracy of our calculated partition coefficients is better than the percentages given above.

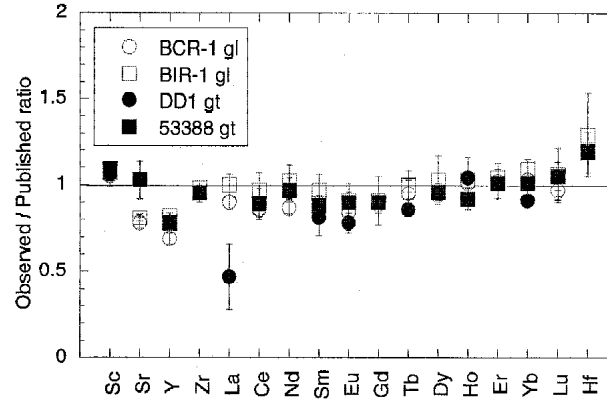

FIGURE 2. Comparison of observed and published values for secondary garnet/glass standards. Data taken from Table 3. Deviation of La in DD1 caused by very low concentration (0.03 ppm according to Irving and Frey 1978), close to the detection limit of the ion microprobe. Observed/published ratio (Obs/Pub) for Sr is always higher in garnet standards than in glass standards, implying that our Sr partition coefficients might be overestimated. Obs/Pub data for Y in glass BIR-1 is lower than Obs/Pub in glass BCR-1, which might be caused by a small error in the published Y content of BIR-1 (Jochum et al. 1990). All of our analyses were calibrated against recommended values for NIST SRM610.

RESULTS AND DISCUSSION

Experimental products and their compositions are listed in Tables 2 and 4, respectively. All experiments produced several homogeneous garnets with a maximum diameter of about 30 μm. Experiments 8 and 11 produced minor orthopyroxene (<5 μm in diameter; unsuitable for SIMS analysis). Experiment 11 (see Fig. 3) produced both glass and quench crystals, whereas all other runs produced quench crystals only. Figure 3 illus-

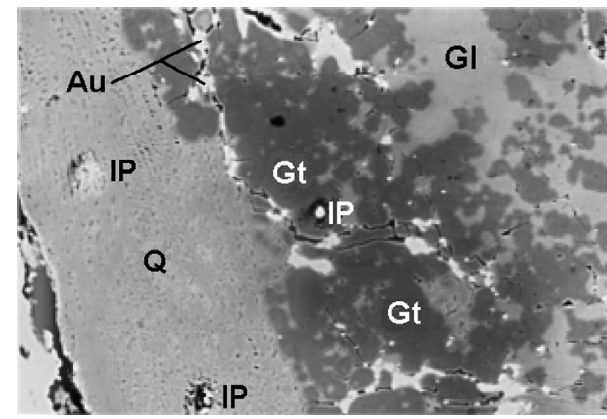

FIGURE 3. Backscattered electron image of experiment 11 showing garnet (Gt), quench (Q), glass (G), gold coating (Au), and ion microprobe pits (IP). (Width of view = 350 μm.)

trates the spinifex texture of the quench crystals. Major and trace element compositions of glass and quench crystals in experiment 11 are indistinguishable, except for boron, which is significantly higher in the latter. This is probably due to surface contamination in the cracks between the quench crystals and in this case, values from the glass were used to calculate *D*. We observed no significant heterogeneity in any of our garnet or quench phases for any of the trace elements, as illustrated by the small relative errors given in Table 4.

Experiments 8 and 11 were performed at very similar conditions and used the same starting material, but the platinum capsule in experiment 8 was not graphite-lined. Direct comparison between the experiments is hampered for some elements by the influence of small amount of surface and/or glass contamination in some garnet analyses (e.g., B, Li, Sr, and La, see later discussion). Inhomogeneity of the starting material for some elements (K, Zr, and Th), which had to be doped to high levels, manifests itself in relatively large differences in absolute concentrations between the two experiments, although in the case of Zr and Th calculated partition coefficients are virtually the same. For other elements (Cd, Ta, In, and Nb) it is obvious from anomalously low concentrations in the quench phase that alloying with the platinum capsule has taken place in experiment 8. (Note that In and Nb were completely lost from this experiment and are therefore absent from Table 4.) Hence, partition coefficients for K, Cd, Ta, In, and Nb calculated for experiment 8 are not included in Table 5. On the other hand, agreement between the REE data for experiments 8 and 11 is very good, warranting the inclusion of REE partitioning data for experiment 8 in later discussion.

Major element compositions of the garnets span a large part of the pyrope-grossular join, ranging from Py_9Gr_{91} (experiment 13) to $Py_{84}Gr_{16}$ (experiment 11). Calculated garnet/melt partition coefficients (Table 5) are summarized in Figure 4a, showing the large variation in *D* along the join. As expected, partition coefficients for Py_{60} and Py_{65} are very similar, as are *D*-values for Py_{82} and Py_{84}. More importantly, partition coefficients for highly incompatible elements such as LREE, Sr and Li vary by more than 2 orders of magnitude along the join from Py_{84} to Py_9. On the other hand, HREE like Yb and Lu show relatively little variation with garnet composition. The existing garnet-melt partitioning data do not cover a wide enough range in garnet composition to observe these effects. However, Harte and Kirkley (1997), in their study of eclogite xenoliths from the Roberts Victor kimberlite pipe in South Africa, provided data on garnet-clinopyroxene partition coefficients ($D^{Gt/Cpx}$) as a function of garnet composition in the range from Gr_8 to Gr_{50}.

TABLE 3. Comparison of observed and published trace element contents of SIMS secondary standards

	Observed / Published ratio			
Element	BCR-1 gl	BIR-1 gl	DD1 gt	53388 gt
Sc	1.05(6)	1.08(2)	1.06(2)	1.09(1)
Sr	0.78(3)	0.81(2)		1.03(11)
Y	0.69(3)	0.82(2)		0.78(2)
Zr	0.95(4)	0.98(4)		0.95(5)
La	0.90(4)	1.00(6)	0.47(19)	
Ce	0.86(5)	0.97(10)		0.89(9)
Nd	0.87(5)	1.02(9)		0.97(7)
Sm	0.89(5)	0.97(9)	0.81(10)	0.88(6)
Eu	0.84(12)	0.91(10)	0.78(2)	0.90(6)
Gd	0.89(5)	0.91(14)		0.90(3)
Tb	0.95(8)	1.00(8)	0.86(3)	
Dy	0.94(4)	1.03(14)		0.96(5)
Ho	1.01(15)	1.03(5)	1.04(3)	0.92(6)
Er	1.02(10)	1.04(5)		1.01(4)
Yb	1.03(3)	1.09(6)	0.91(4)	1.01(6)
Lu	0.97(7)	1.06(15)		1.05(8)
Hf		1.29(24)		1.19(12)

Note: Observed compositions from analyses by W.v.W. and J.DB. in the period 1993–1997; published values from Govindaraju (1994; BCR-1), Jochum et al. (1990, BIR-1), Irving and Frey (1978; DD1) and Norman et al. (1996; MU53388) Observed/published ratios are given for elements measured at least twice by both W.v.W. and J.D.B.

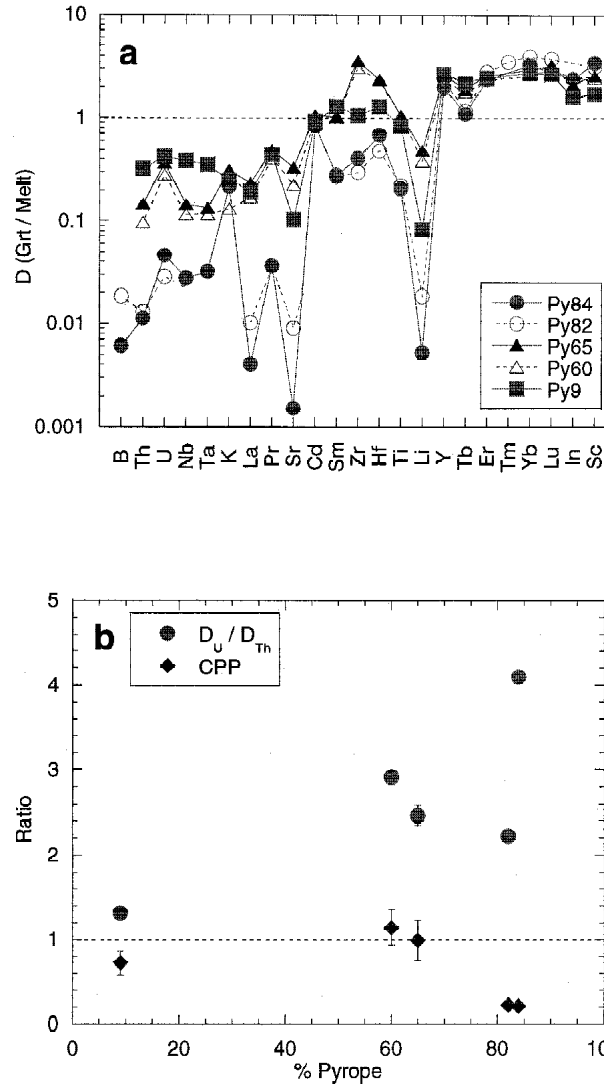

FIGURE 4. (a) Spidergram showing garnet/melt partition coefficients from this study. Order of elements along x-axis (where possible) from Sun and McDonough (1989). In and Li after Withers (1997). Note large variation in *D*-values with garnet composition for some elements (e.g., LREE, Sr, Li, and HFSE). **(b)** Variation of D_U/D_{Th} and CPP (Critical Partitioning Parameter—Hart and Dunn 1993) along pyrope-grossular join. Error bars are ±1σ.

TABLE 4. Major and trace element composition of experimental products

	8				11				12				13			
Elements	Grt	σ	Q	σ	Grt	σ	Gl	σ	Grt	σ	Q	σ	Grt	σ	Q	σ
CaO	7.5	1.1	14.2	1.4	6.7	0.4	15.2	0.3	14.2	1	21.9	0.9	34.7	1.0	26.6	1.2
MgO	24.6	0.6	22.0	1.4	25.1	0.3	19.9	0.3	19.1	0.3	12.5	0.7	2.5	0.6	7.2	0.9
Al_2O_3	23.7	1.2	15.2	1.5	25.0	1.2	15.9	0.2	23.9	0.3	21.9	1.1	23.3	0.4	26.1	2.2
SiO_2	44.1	0.9	48.4	0.9	44.7	1.0	48.9	0.4	44.1	0.4	43.7	0.8	41.0	0.3	40.4	1.1
Total	99.9	1.0	99.8	1.0	102	0.4	99.8	0.5	101	0.4	100	0.6	101	0.6	100	1.0
n (majors)	31		9		46		16		3		10		19		20	
Li	0.7	0.1	39	2	0.05	0.01	10	1	6.5	0.7	14	1	1.2	0.03	15	
B	11	3	589	45	3.6	0.4	599	27								
K	20	14	3853	646	375	11	1731	178	435	13	1394	120	177	0.3	707	
Sc	26	0.6	8.3	0.2	24	2	7.0	0.1	22	1	8.4	0.8	27	1	16	
Ti	10	0.5	46	6	13	0.8	64	7	24	1	23	2	24	1	29	
Sr	2.3	0.7	255	28	0.37	0.05	241	13	62	1	188	17	62	5	600	
Y	11	0.5	4.7	0.1	11	0.7	5.5	0.08	22	2	8.5	0.6	29	5	11	
Zr	45	4	152	10	13	0.7	32.1	0.4	22	0.2	6.2	0.4	27	0.6	25	
Nb					0.87	0.06	31	1	4.6	0.07	32	5	11	0.2	29	
Cd	67	29	20	3	107	4	129	10	108	5	102	8	15	0.1	17	
In					246	11	102	2	433	31	205	38	18	0.4	11	
La	1.1	0.3	106	10	0.38	0.02	94	3	9.9	0.3	42	5	18	3	93	
Pr	1.0	0.2	27	2	0.88	0.03	24.2	0.4	5.8	0.06	12	1	11	1	25	
Sm	3.8	0.1	14	0.8	3.8	0.3	13.7	0.6	10.6	0.01	11	0.6	22	0.5	17	
Tb	10	0.8	8.6	0.3	9.9	0.6	9.0	0.1	15	1	7.6	0.3	19	2	8.7	
Er	15	1	5.5	0.4	14	1	5.9	0.2	16	2	6.3	0.5	62	13	25	
Tm	16	2	4.5	0.06												
Yb	15	2	4.0	0.1	13	1	4.1	0.2	15	2	5.2	0.7	22	5	7.9	
Lu	7	3	1.9	0.1	7.3	0.7	1.3	0.8	16	2	5.0	0.6	23	4	8.9	
Hf	6.4	0.5	13	1	7.8	0.6	12	0.5	12	1	5.1	0.4	16	0.2	12	
Ta	13	5	25	3	18	2	563	16	3.9	0.1	29	5	15	2	42	
Th	23	5	1753	188	16	2	1421	39	99	0.3	671	49	49	5	153	
U	8	2	286	41	12	1	249	10	49	5	136	13	20	0.1	46	
n (traces)	4		4		6		8		2		5		2		1	

Note: Major elements in weight percent, trace elements in parts per million. Grt = Garnet, Q = Quench phase, Gl = Glass phase.

They observed an increase by up to three orders of magnitude in $D_{\mathrm{LREE}}^{\mathrm{Gt/Cpx}}$ with increasing grossular content, while $D_{\mathrm{HREE}}^{\mathrm{Gt/Cpx}}$ remained approximately constant. This is consistent with our experimental results (Fig. 4a). Several trace elements listed in Table 5 have not been used before in garnet-melt partitioning studies. Lithium is consistently more incompatible than the HREE, confirming the expectations of Ryan and Langmuir (1987). Figure 4a also shows that In is compatible in garnet (D_{In} ~2), while D_{Cd} is about unity for most experiments. Boron is highly incompatible, with D_{B} similar to D_{La} (Table 5). Finally, Pr is incompatible with $D_{\mathrm{La}} < D_{\mathrm{Pr}} < D_{\mathrm{Sm}}$.

Parameters deemed important for mantle melting also show remarkable variation along the pyrope-grossular join. For example, Figure 4b shows the large change in $D_{\mathrm{U}}/D_{\mathrm{Th}}$ with garnet composition (from 4.1 for Py_{84} to only 1.3 for Py_9). Values for the Critical Partitioning Parameter (CPP = $[D_{\mathrm{Sm}}\, D_{\mathrm{Hf}}]/[D_{\mathrm{Nd}}\, D_{\mathrm{Lu}}]$) from Hart and Dunn (1993) are also shown in Figure 4b. Values of CPP give a measure of the extent of fractionation of the Sm/Nd and Lu/Hf isotopic systems, and the fact that mantle garnets have a low CPP has been used to infer that MORB melting needs to start in the garnet lherzolite stability field (e.g., Salters and Hart 1989). The CPP values for Py_{82} and Py_{84} are very close to the value of 0.18 used by Salters (1996) in his modeling of MORB generation. However, other garnets show values much closer to or even greater than 1, similar to the value calculated for the garnet from the experiment of Hauri et al. (1994; CPP = 0.97) and, more significantly, similar to CPP values for clinopyroxene (Blundy et al. 1998).

To interpret the compositional dependence of trace element partitioning seen in Figure 4, we used the crystal-melt partitioning model of Blundy and Wood (1994), as extended by Wood and Blundy (1997). This model is based on the long-established observation (e.g., Onuma et al. 1968) that mineral-melt partition coefficients for series of isovalent cations show a near-parabolic dependence on cation radius. This has been shown for plagioclase (Blundy and Wood 1991), amphibole (e.g., Liu et al. 1992; LaTourrette et al. 1995; Brenan et al. 1995), clinopyroxene (Blundy et al. 1995; Wood and Blundy 1997), olivine (Beattie 1994), and garnet (Liu et al. 1992; Van Westrenen et al. 1997; Withers 1997). Beattie (1994) and Blundy and Wood (1994) explained these observations using lattice strain models, based on the work of Nagasawa (1966) and Brice (1975), respectively. In the model of Blundy and Wood (1994), trace element partitioning on a given structural site is characterized by the site radius (r_0), its Young's modulus (E), and the (theoretical) strain-free partition coefficient D_0 for an element with "ideal" radius r_0:

$$D_i = D_0 \exp\left[\frac{-4\pi E N_A \left[\frac{r_0}{2}(r_i - r_0)^2 + \frac{1}{3}(r_i - r_0)^3\right]}{RT}\right] \quad (1)$$

N_A is Avogadro's number, R is the gas constant, and T is in K. Wood and Blundy (1997) used this model to predict REE D-values for clinopyroxene-melt partitioning, and Van Westrenen et al. (1997) concluded from a study of available literature data that this model is also applicable to garnet-melt partitioning of trace elements.

We used a Levenberg-Marquardt-type, non-linear least-squares fitting routine (Press et al. 1992) to derive best-fit val-

TABLE 4.—*Extended.*

	14			
Elements	Grt	σ	Q	σ
CaO	15.8	0.4	21.4	0.7
MgO	17.3	0.4	12.9	0.6
Al_2O_3	23.3	0.5	21.7	0.9
SiO_2	43.6	0.3	43.7	0.7
Total	100	0.4	99.7	0.4
n (majors)	7		17	
Li	5.9	0.9	15	0.4
B				
K	269	10	2068	209
Sc	24	2	9.6	0.9
Ti	21	0.5	20	1
Sr	51	7	227	12
Y	23	1	9.8	0.5
Zr	25	3	8.2	0.7
Nb	6.7	0.7	58	5
Cd	105	7	105	13
In	417	23	166	20
La	9.9	1	58	4
Pr	5.6	0.3	14	0.5
Sm	11	0.2	10	0.6
Tb	14	0.7	8.1	0.4
Er	17	0.6	7.3	0.6
Tm				
Yb	17	1	6.5	0.4
Lu	18	1	6.2	0.5
Hf	16	0.1	7.0	0.8
Ta	7.9	0.6	68	4
Th	146	16	1506	92
U	80	5	282	20
n (traces)	3		4	

ues for r_0, D_0, and E for partitioning of the large ($r_i \geq 0.89$ Å) 3+ cations (REE, Y, In, and Sc). Trivalent cations were chosen as the basis of these fits because these form the largest group of isovalent trace elements in our experiments. Their D-values should, therefore, provide the tightest constraints on partitioning behavior. Standard deviations of multiple analyses from Table 5 were used to weight the fits. The following additional constraints and assumptions were applied.

•The REE and Y all partition exclusively into the garnet X-site. Recent EXAFS studies (Quartieri et al. 1997) and initial studies of garnet/melt partitioning (Van Westrenen et al. 1997; Withers 1997) support this assumption.

•Indium can be univalent or trivalent. Since garnet-melt partition coefficients for 1+ cations (K and Li) are about two orders of magnitude smaller than D-values for 3+ cations (see Fig. 4a), small amounts of In^{1+} should lead to a significant lowering of observed D_{In} relative to a 3+ ion of the same radius. Fitted values for D_{In3+} should therefore generally be higher than observed D_{In}.

•Sc can enter both the garnet X- and Y-sites (e.g., Geller 1967). Sc entering the Y-site has been observed by several authors (see Geller 1967) but, because of its ionic radius (0.89 Å according to Shannon 1976) and in the absence of other (e.g., EXAFS) data, we expect some of the Sc to enter the X-site. With Sc entering both sites, fitted D_{Sc} should underestimate the observed D_{Sc}.

Table 6 gives our best-fit values for r_0, D_0, and E. Plots of ionic radius vs. D using these parameters (Fig. 5) show good agreement between observation and model for all experiments, bearing in mind the assumptions listed above. Deviations of our fitted values from the measured partition coefficients for La and Pr are probably caused by slight (~0.5%) contamination of garnet by glass during SIMS analysis. As illustrated in Figure 6a, fitted values of r_0 vary systematically with garnet

TABLE 5. Garnet-melt partition coefficients

	8 (Py82)		11 (Py84)		12 (Py65)		13 (Py9)		14 (Py60)	
Element	*D*	σ	*D*	σ	*D*	σ	*D*	σ	*D*	σ
Ca	0.53	0.09	0.44	0.03	0.65	0.05	1.3	0.07	0.74	0.03
Mg	1.1	0.1	1.3	0.03	1.5	0.08	0.34	0.1	1.3	0.07
Al	1.6	0.2	1.6	0.08	1.1	0.06	0.89	0.08	1.1	0.05
Si	0.91	0.02	0.91	0.02	1.0	0.02	1.0	0.03	1.0	0.02
Li	0.018	0.002	0.0052	0.0007	0.48	0.07	0.083	0.002	0.38	0.06
B	0.018	0.003	0.0060	0.0006						
K			0.22	0.02	0.31	0.03	0.25	0.0004	0.13	0.01
Sc	3.1	0.1	3.4	0.2	2.6	0.3	1.7	0.1	2.4	0.3
Ti	0.2	0.01	0.2	0.02	1.1	0.1	0.8	0.04	1.0	0.06
Sr	0.009	0.002	0.002	0.0002	0.3	0.03	0.1	0.01	0.2	0.03
Y	2.4	0.07	2.0	0.1	2.6	0.3	2.7	0.4	2.3	0.2
Zr	0.3	0.02	0.4	0.02	3.6	0.2	1.1	0.02	3.1	0.4
Nb			0.03	0.002	0.2	0.02	0.4	0.01	0.1	0.02
Cd			0.8	0.07	1.1	0.1	0.9	0.01	1.0	0.1
In			2.4	0.1	2.1	0.4	1.6	0.04	2.5	0.3
La	0.010	0.002	0.0040	0.0002	0.24	0.03	0.19	0.03	0.17	0.02
Pr	0.036	0.004	0.036	0.001	0.48	0.05	0.44	0.05	0.40	0.03
Sm	0.27	0.01	0.28	0.02	1.0	0.06	1.3	0.03	1.0	0.1
Tb	1.2	0.05	1.1	0.06	1.9	0.2	2.2	0.3	1.8	0.1
Er	2.8	0.2	2.4	0.2	2.6	0.4	2.5	0.5	2.4	0.2
Tm	3.5	0.2								
Yb	3.9	0.2	3.3	0.3	2.9	0.6	2.8	0.7	2.6	0.2
Lu	3.7	0.7	5.7	0.5	3.2	0.6	2.7	0.5	2.9	0.3
Hf	0.48	0.03	0.68	0.06	2.4	0.3	1.3	0.02	2.3	0.3
Ta			0.032	0.003	0.13	0.02	0.35	0.04	0.12	0.01
Th	0.013	0.002	0.011	0.001	0.15	0.01	0.32	0.03	0.10	0.01
U	0.029	0.004	0.046	0.004	0.36	0.05	0.42	0.002	0.28	0.03

Note: All values calculated using data in Table 4.

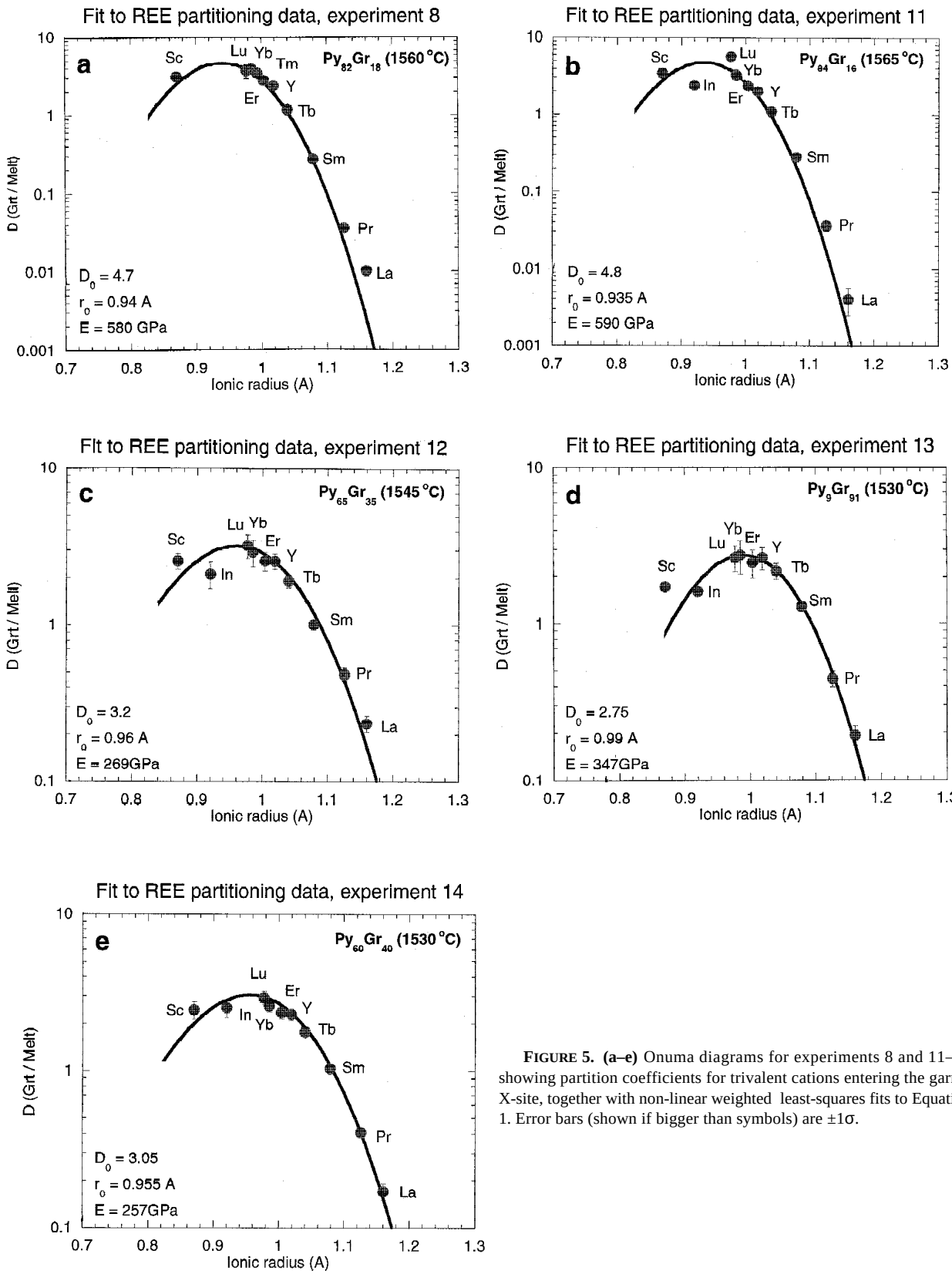

FIGURE 5. (a–e) Onuma diagrams for experiments 8 and 11–14 showing partition coefficients for trivalent cations entering the garnet X-site, together with non-linear weighted least-squares fits to Equation 1. Error bars (shown if bigger than symbols) are ±1σ.

TABLE 6. Results of fitting of partitioning data for Y, REE, In, and Sc to Equation 1

Experiment	Composition	r_0	σ	D_0	σ	E	σ
8	$Py_{82}Gr_{18}$	0.940	0.005	4.7	0.1	580	40
11	$Py_{84}Gr_{16}$	0.935	0.004	4.8	0.1	590	40
12	$Py_{65}Gr_{35}$	0.960	0.008	3.2	0.3	269	17
13	$Py_{9}Gr_{91}$	0.99	0.01	2.8	0.1	347	20
14	$Py_{60}Gr_{40}$	0.955	0.008	3.1	0.1	257	20

Note: r_0 in Å, E in GPa.

composition. Linear regression of r_0 against garnet composition gives

$$r_0 = 0.993 - 0.0628\,X_{Py}\ \text{Å} \quad (2)$$

Figure 6a also shows variations in crystallographic measurements of the size of the garnet X-site with major element composition. Garnet X-sites are not cubic; there are two nonequivalent sets of four bond distances around the divalent cation leading to a range in X-site radii, shown as the grey area in Figure 6a. X-site radii for pure pyrope and pure grossular, predicted from the partitioning data using Equation 2 (0.930 Å and 0.993 Å respectively), are well within the range of radii derived from crystallographic measurements. We conclude that values of r_0 determined from fits to the trace element data are a good approximation of the true variation in the effective radius of the garnet X-site. Although beyond the scope of this paper, this direct relationship probably extends to natural situations (i.e., garnets containing significant amounts of Fe, Mn, and/or Cr), as is the case for clinopyroxene (see Wood and Blundy 1997).

Figure 6b displays the variation of D_0 with garnet composition. D_0 is influenced by small variations in temperature as well as crystal and melt composition. Van Westrenen et al. (1997) showed that D_0 generally increases with decreasing temperature, partly due to the high enthalpies of fusion of end-member garnets. In the present study, however, the pyrope-rich garnets, synthesized at 1560–1565 °C, have a higher D_0 than the more grossular-rich garnets formed at temperatures of 1530–1545 °C. This difference in D_0 is a reflection of the importance of configurational entropy effects in both crystal and melt (Blundy et al. 1996). Configurational effects are anticipated in this study, because of the very large compositional range of our garnet crystals and melts. Specifically, the higher D_0 values for Py_{82} and Py_{84} are a consequence of the fact that the melts in these experiments are *not* on the pyrope-grossular join, as opposed to the melts in the other experiments. Quantification of these effects requires application of activity-composition relations for both garnet and melt, which is beyond the scope of this study.

Finally, let us consider our derived values of Young's modulus (E). Blundy and Wood (1994) and Wood and Blundy (1997) showed that derived E values for plagioclase/melt and clinopyroxene/melt partitioning of 1+, 2+, and 3+ cations can be rationalized using the relationships established by Anderson and Anderson (1970) and extended by Hazen and Finger (1979). Anderson and Anderson (1970) showed that the bulk moduli (K) of many different oxides depend linearly on cation charge (Z_c) and are inversely proportional to molecular volume V_0:

$$K = 15.7(\pm 0.5)\frac{Z_c Z_o}{V_0}\ \text{GPa} \quad (3)$$

where Z_o is the charge on the oxygen anion. Hazen and Finger (1979) extended this work to cations coordinated by oxygen in silicates and oxides and, using the fact that V_0 is approximately equal to the interatomic (cation-oxygen) distance cubed (d^3), they obtained

$$K = 15.7(\pm 0.5)\frac{Z_c Z_o}{V_0}\ \text{GPa} \quad (4)$$

with d in Å. By using the identities $E = 3K(1 - 2\sigma)$ (with σ, Poisson's ratio, taken as 0.25) and $r_0 + r_{oxygen} = d$ (with r_{oxygen} = 1.38 Å after Shannon 1976), best-fit values for E and r_0 can be compared with mineral physics data represented by Equation 4. Figure 7 is a plot of bulk modulus (K) vs. Z_c/d^3, and shows

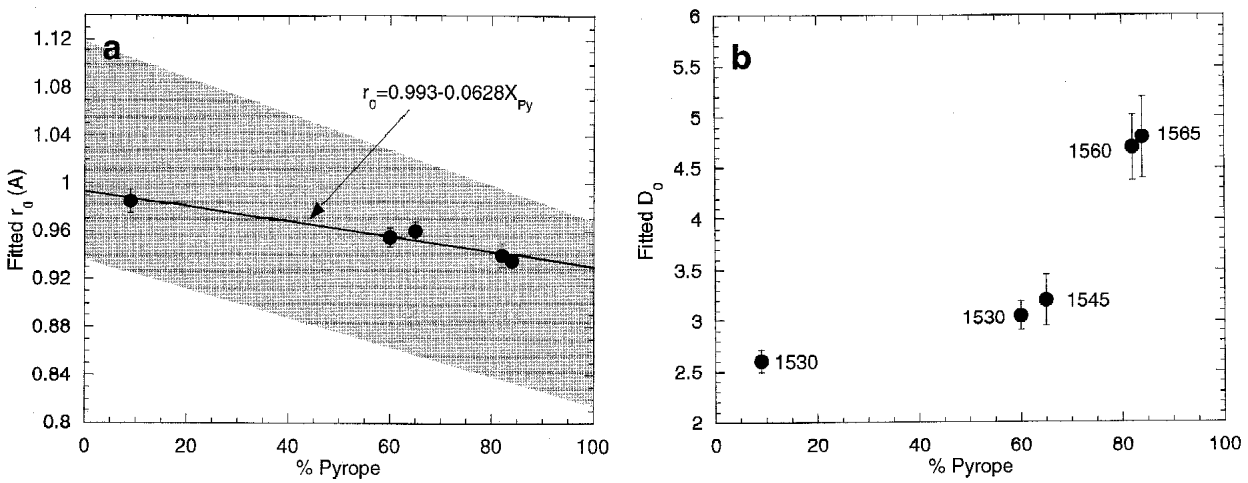

FIGURE 6. (a) Variation of r_0 along the pyrope-grossular join. Error bars are ±1s. Solid line is a linear fit to r_0 data from Table 6. Shaded area shows expected variation in X-site radius in pyrope-grossular solid solutions, taking into account the variations of cation-oxygen distances around the end-member X-sites taken from Smyth and Bish (1988), and using r_{oxygen} = 1.38 Å. **(b)** Variation of D_0 along pyrope-grossular join. Error bars are ±1σ. T (in °C) is shown adjacent to each point.

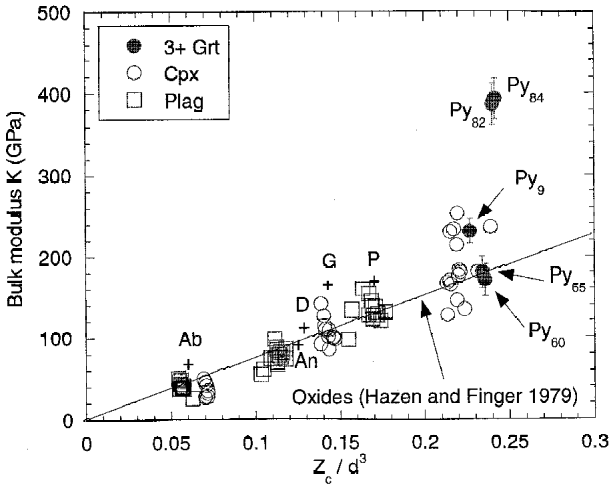

FIGURE 7. Site bulk modulus (K) derived from partitioning experiments vs. cation charge (Z_c) over metal-oxygen distance cubed (d^3) for univalent, divalent, and trivalent cations in plagioclase and the clinopyroxene M2 site (Blundy and Wood 1994; Wood and Blundy 1997), and trivalent cations in garnet (this study; error bars are ±1s). Note the divergence at higher Z_c/d^3 values from the linear relationship derived by Hazen and Finger (1979) for cation polyhedra in oxides. Crosses show bulk moduli of end-member minerals albite (Ab), anorthite (An), diopside (D), grossular (G), and pyrope (P). Adapted from Wood and Blundy (1997).

the curve defined by Equation 4 together with data from Blundy and Wood (1994) and Wood and Blundy (1997), and our garnet-melt data from Table 6. It is clear from Figure 7 that our new data extend the range seen for clinopyroxene-melt partitioning to higher values of K. It is also apparent that a large positive deviation from the Hazen and Finger relation occurs at higher values of Z_c/d^3. Furthermore, the X-sites in both our pyrope-rich (Py_{84} and Py_{82}) and grossular-rich (Py_9) garnets appear stiffer than our intermediate (Py_{65} and Py_{60}) garnets.

With respect to the high values of K for pyrope-rich garnets, it is well-documented that pyrope does not follow the Hazen and Finger relation (e.g., Leger et al. 1990; Olijnyk et al. 1991). The published data, however, show pyropic garnets to be *less* compressible than grossular, but this is not the case in our experiments (Fig. 7). The high values of K derived for pyrope-rich garnets from this study are not unique: fitting of Equation 1 to other well-constrained experimental garnet-melt partitioning data with similar high values of Z_c/d^3 (Hauri et al. 1994; Withers 1997) gives K values in the range of 390–450 GPa. Furthermore, preliminary static lattice energy simulations (Van Westrenen et al. 1998) of the incorporation of trivalent defects into pyrope X-sites, show the same high values for K. At present we have no satisfactory explanation for this phenomenon, although the heterovalent nature of the substitution, and consequent requirement for charge balance through coupled substitution, is probably an important factor.

On the other hand, our observations on the non-linearity of K along the pyrope-grossular join are particularly relevant in light of the IR powder absorption spectroscopic study on garnets along the same join by Boffa Ballaran et al. (unpublished manuscript). Their data show a pronounced softening of low-frequency IR modes in intermediate pyrope-grossular garnets. According to Boffa Ballaran et al. (unpublished manuscript), this mode softening could be a result of an incipient phase transition in intermediate pyrope-grossular garnets caused by local structural heterogeneities. Carpenter and Salje (1998) pointed out that close to phase transition points elastic constants can go to zero, or at least become very small. This "softening" of structures close to phase transition points is consistent with the lower values of E observed for intermediate pyrope-grossular garnets in our experiments (Fig. 7), and reinforces our proposal that trace element partitioning experiments can provide structural information relevant to mineral physics.

With respect to a garnet-melt partitioning model, it is therefore not viable to constrain E in Equation 1 by the Hazen and Finger relationship (Eq. 4). Future work needs to focus on finding a more general relationship between K, Z_c, and d that is valid for garnet and other relatively incompressible phases (i.e., at relatively high values of Z_c/d^3). It should then be possible to put tighter constraints on E for univalent and divalent cations. Without these constraints, fitting Equation 1 to partitioning data for these cations is difficult because of the small number of elements present in our experiments. Partition coefficients for 4+ cations (Zr, Hf, Ti, U, and Th) do not show the regular pattern in $D - r$ space observed for the trivalent cations. This is related to the fact that these elements enter sites other than the X-site (e.g., Ti^{4+} goes mainly into the Z-site), so that observed D-values are a sum of D-values on the two sites. We have, therefore, made no attempt to fit 4+ D-values to Equation 1.

Although our experiments were done in a simple system and exhibit a wide compositional range, we argue that our results have important implications for garnet/melt partitioning in natural systems. In mantle garnets (i.e., garnets from garnet peridotites and group-A eclogites), generally over 60–90% of the X-site is occupied by Mg and Ca, the other 10–40% taken up by Fe^{2+} and Mn^{2+} and, in the case of depleted mantle rocks, Cr^{3+} (e.g., Mottana 1986). The compositional variation of mantle garnets, combined with the significant effects of composition on partitioning seen in this study call into question any mantle melting model using fixed and constant garnet-melt partition coefficients.

ACKNOWLEDGMENTS

Many thanks to Stuart Kearns, Richard Hinton, and John Craven for all their help during EMPA and SIMS analysis, and to Fred Wheeler, Mike Dury, and Paul Simon for technical assistance. This paper benefited greatly from thorough and critical reviews of C. Geiger and T. LaTourrette, comments by W. McDonough and an anonymous reviewer, discussions with M. Carpenter, and access to unpublished work by T. Boffa Ballaran. W.v.W. acknowledges Dutch VSB Foundation, NERC, and EU (contract ERBFMBICT 971991) for financial support. J.D.B. thanks the Royal Society for a Research Fellowship.

REFERENCES CITED

Anderson, D.L. and Anderson, O.L. (1970) The bulk modulus-volume relationship for oxides. Journal of Geophysical Research, 75, 3494–3500.

Beattie, P. (1993) Uranium-thorium disequilibria and partitioning on melting of garnet peridotite. Nature, 363, 63–65.

——— (1994) Systematics and energetics of trace-element partitioning between olivine and silicate melts: Implications for the nature of mineral/melt partitioning. Chemical Geology, 117, 57–71.

Blundy, J.D. and Brodie, J. (1997) Modelling mantle melting with variable partition coefficients. Lunar and Planetary Institution Contribution, 921, 30–31.

Blundy, J.D. and Wood, B.J. (1991) Crystal-chemical controls on the partitioning of

Sr and Ba between plagioclase feldspar, silicate melts and hydrothermal solutions. Geochimica et Cosmochimica Acta, 55, 193–209.

——— (1994) Prediction of crystal-melt partition coefficients from elastic moduli. Nature, 372, 452–454.

Blundy, J.D., Falloon, T.J., Wood, B.J., and Dalton, J.A. (1995) Sodium partitioning between clinopyroxene and silicate melts. Journal of Geophysical Research, 100, 15501–15515.

Blundy, J.D., Wood, B.J., and Davies, A. (1996) Thermodynamics of rare earth element partitioning between clinopyroxene and melt in the system CaO-MgO-Al_2O_3-SiO_2. Geochimica et Cosmochimica Acta, 60, 359–364.

Blundy, J.D., Robinson, J.A.C., and Wood, B.J. (1998) Heavy REE are compatible in clinopyroxene on the spinel lherzolite solidus. Earth and Planetary Science Letters, 160, 493–504.

Brenan, J.M., Shaw, H.F., Ryerson, F.J., and Phinney, D.L. (1995) Experimental determination of trace-element partitioning between pargasite and a synthetic hydrous andesitic melt. Earth and Planetary Science Letters, 135, 1–11.

Brice, J.C. (1975) Some thermodynamic aspects of the growth of strained crystals. Journal of Crystal Growth, 28, 249–253.

Carpenter, M.A. and Salje, E.K.H. (1998) Elastic anomalies in minerals due to structural phase transitions. European Journal of Mineralogy, 10, 693–812.

Frost, D.J. and Wood, B.J. (1997) Experimental measurements of the fugacity of CO_2 and graphite/diamond stability from 35 to 77 kbar at 925 to 1650°C. Geochimica et Cosmochimica Acta, 61, 1565–1574.

Geller, S. (1967) Crystal chemistry of the garnets. Zeitschrift für Kristallographie, 125, 1–47.

Govindaraju, K. (1994) 1994 compilation of working values and sample description for 383 geostandards. Geostandards Newsletter, 18, 1–158.

Hart, S.R. and Dunn, T. (1993) Experimental cpx/melt partitioning of 24 trace elements. Contributions to Mineralogy and Petrology, 113, 1–8.

Harte, B. and Kirkley, M.B. (1997) Partitioning of trace elements between clinopyroxene and garnet: data from mantle eclogites. Chemical Geology, 136, 1–24.

Hauri, E.H., Wagner, T.P., and Grove, T.L. (1994) Experimental and natural partitioning of Th, U, Pb and other trace elements between garnet, clinopyroxene and basaltic melts. Chemical Geology, 117, 149–166.

Hazen, R.M. and Finger, L.W. (1979) Bulk modulus-volume relationship for cation-anion polyhedra. Journal of Geophysical Research, 84, 6723–6728.

Irving, A.J. and Frey, F.A. (1978) Distribution of trace elements between garnet megacrysts and host volcanic liquids of kimberlitic to rhyolitic composition. Geochimica et Cosmochimica Acta, 42, 771–787.

Jochum, K.P., Seufert, H.M., and Thirlwall, M.F. (1990) Multi-element analysis of 15 international standard rocks by isotope-dilution sparks source mass spectrometry. Geostandards Newsletter, 14, 469–473.

LaTourrette, T.Z., Kennedy, A.K., and Wasserburg, G.J. (1993) Thorium-Uranium fractionation by garnet: Evidence for a deep source and rapid rise of oceanic basalts. Science, 261, 739–742.

LaTourrette, T.Z., Hervig, R.L., and Holloway, J.R. (1995) Trace element partitioning between amphibole, phlogopite, and basanite melt. Earth and Planetary Science Letters, 135, 13–30.

Leger, J.M., Redon, A.M., and Chateau, C. (1990) Compressions of synthetic pyrope, spessartine and uvarovite garnets up to 25 GPa. Physics and Chemistry of Minerals, 17, 161–167.

Liu, C.-Q., Masuda, A., Shimizu, H., Takahashi, K., and Xie, G.-H. (1992) Evidence for pressure dependence of the peak position in the REE mineral/melt partition patterns of clinopyroxene. Geochimica et Cosmochimica Acta, 56, 1523–1530.

Maaløe, S. and Wyllie, P.J. (1979) The join grossularite-pyrope at 30kb and its petrological significance. American Journal of Science, 279, 288–301.

Mottana, A. (1986) Crystal-chemical evaluation of garnet and omphacite microprobe analyses: its bearing on the classification of eclogites. Lithos, 19, 171–186.

Nagasawa, H. (1966) Trace element partition coefficient in ionic crystals. Science, 152, 767–769.

Norman, M.D., Pearson, N.J., Sharma, A., and Griffin, W.L. (1996) Quantitative analysis of trace elements in geological materials by Laser Ablation ICPMS: Instrumental operating conditions and calibration values of NIST glasses. Geostandards Newsletter, 20, 247–261.

Olijnyk, H., Paris, E., Geiger, C.A., and Lager, G.A. (1991) Compressional study of katoite [$Ca_3Al_2(O_4H_4)_3$] and grossular garnet. Journal of Geophysical Research, 96, 14313–14318.

Onuma, N., Higuchi, H., Wakita, H., and Nagasawa, H. (1968) Trace element partition between two pyroxenes and the host lava. Earth and Planetary Science Letters, 5, 47–51.

Perkins III, D., Holland, T.J.B., and Newton, R.C. (1981) The Al_2O_3 contents of enstatite in equilibrium with garnet in the system MgO-Al_2O_3-SiO_2 at 15–40 kbar and 900–1600 °C. Contributions to Mineralogy and Petrology, 78, 99–109.

Press, W.H., Teukolsky, S.A., Vetterling, W.T., and Flannery, B.P. (1992) Numerical Recipes in C, 2nd ed., Cambridge University Press, 965 p.

Quartieri, S., Antonioli, G., Geiger, C.A., and Artioli, G. (1997) EXAFS determination of the structural site of Yb in synthetic pyrope and grossular garnets. Terra Abstracts, 9, 428.

Reed, W.P. (1992) Certificate of analysis: Standard Reference Materials 610 and 611. National Institute of Standards and Technology, 1–3.

Ryan, J.G. and Langmuir, C.H. (1987) The systematics of lithium abundances in young volcanic rocks. Geochimica et Cosmochimica Acta, 51, 1727–1741.

Salters, V.J.M. (1996) The generation of mid-ocean ridge basalts from the Hf and Nd isotope perspective. Earth and Planetary Science Letters, 141, 109–123.

Salters, V.J.M. and Hart, S.R. (1989) The hafnium paradox and the role of garnet in the source of mid-ocean-ridge basalts. Nature, 342, 420–422.

Shannon, R.D. (1976) Revised effective ionic radii and systematic studies of interatomic distances in halides and chalcogenides. Acta Crystallografica, A32, 751–767.

Smyth, J.R. and Bish, D.L. (1988) Crystal structures and cation sites of the rock-forming minerals, 332 p. Allen & Unwin, Boston.

Sun, S. and McDonough, W.F. (1989) Chemical and isotopic systematics of oceanic basalts: implications for mantle composition and processes. In A. Saunders and M.J. Norry, Magmatism in the ocean basins. Geological Society Special Publication, 42, 313–345.

Van Westrenen, W., Blundy, J.D., Wood, B.J., and Withers, A. (1997) Garnet/melt trace element partitioning: theory and experiment. Terra Abstracts, 9, 452.

Van Westrenen, W., Blundy, J.D., Purton, J.A., and Wood, B.J. (1998) Towards a predictive model for garnet-melt trace element partitioning: experimental and computational results. Mineralogical Magazine, 62A, 1580–1581.

Walter, M.J. and Presnall, D.C. (1994) Melting behavior of simplified lherzolite in the system CaO-MgO-Al_2O_3-SiO_2-Na_2O from 7 to 35 kbar. Journal of Petrology, 35, 329–359.

Withers, A.C. (1997) Water in the mantle, 192 p. PhD Thesis, University of Bristol, U.K.

Wood, B.J. and Blundy, J.D. (1997) A predictive model for rare earth element partitioning between clinopyroxene and anhydrous silicate melt. Contributions to Mineralogy and Petrology, 129, 166–181.

MANUSCRIPT RECEIVED FEBRUARY 13, 1998
MANUSCRIPT ACCEPTED NOVEMBER 15, 1998
PAPER HANDLED BY CHARLES A. GEIGER